Supporting Information

Nanoscale structural dynamics of cell edge in breast tumour cells revealed by scanning ion conductance microscopy

Masahiro Yamazaki[a,b,‡], Linhao Sun[c,‡], Tatsunori Nishimura[a,†], Tsunaki Hongu[a], Shigeyuki Takamatsu[b], Toshifumi Gabata[b], Noriko Gotoh[a,d,*], and Shinji Watanabe[c,*]

[a] Division of Cancer Cell Biology, Cancer Research Institute, Kanazawa University, Kanazawa 920-1192, Japan

[b] Department of Radiology, Kanazawa University, Graduate School of Medical Science, 13-1, Takara-machi, Kanazawa 920-8640, Japan

[c] Nano Life Science Institute (WPI-NanoLSI), Kanazawa University, Kakuma-machi, Kanazawa 920-1192, Japan

[d] Institute for Frontier Science Initiative, Kanazawa University, Kakuma-machi, Kanazawa 920-1192, Japan

[†] Present address: Nagoya University Graduate School of Medicine, 65 Tsurumai-cho, Showa-ku, Nagoya 466-8550, Japan

[‡] Equal contribution to this work.

***Corresponding authors**

Shinji Watanabe: wshinji@se.kanazawa-u.ac.jp

Noriko Gotoh: ngotoh@staff.kanazawa-u.ac.jp

SI-supporting text

I-V curve measurement

The electrical resistance measurements were performed to roughly estimate the pore sizes of nanopipettes based on the empirical equation among cone angle, pore diameter, and resistance[1], where the resistance was calculated from current–voltage measurement. In details, 150 mM KCl filled nanopipettes were immersed into bulk solution of 150 mM KCl in a homemade system. Current amplifier (DLPCA-200 OPTO FEMTO, GMBH Germany) was used to magnify the detected ion current signal. A multifunction generator (WF-1973, NF Corp.) was used to supply a bias voltage between two Ag/AgCl electrodes. An oscilloscope (DSOx1102G, KEYSIGHT TECHNOLOGIES, INC) was utilized to record the input and output voltages.

Transmission electron microscopy (TEM)

The geometrical shape of nanopipettes including pore diameter and conical angle was analyzed by TEM measurement, where the measured condition was described in our previous work[2].The observed nanopipettes had an inner pore size of 40 –50 nm.

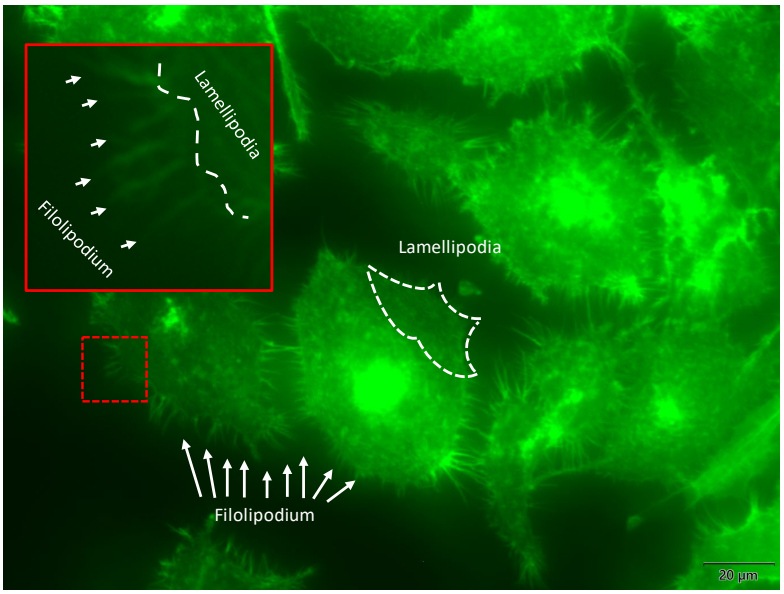

Figure S1 Revealing microstructures from staining breast cancer cells by fluorescence microscopy, including filopodium, lamellipodia and actin filament. Alexa Fluor™ 488 Phalloidin was used for actin filament staining. This image was obtained with OLYMPUS IX83 microscope system.

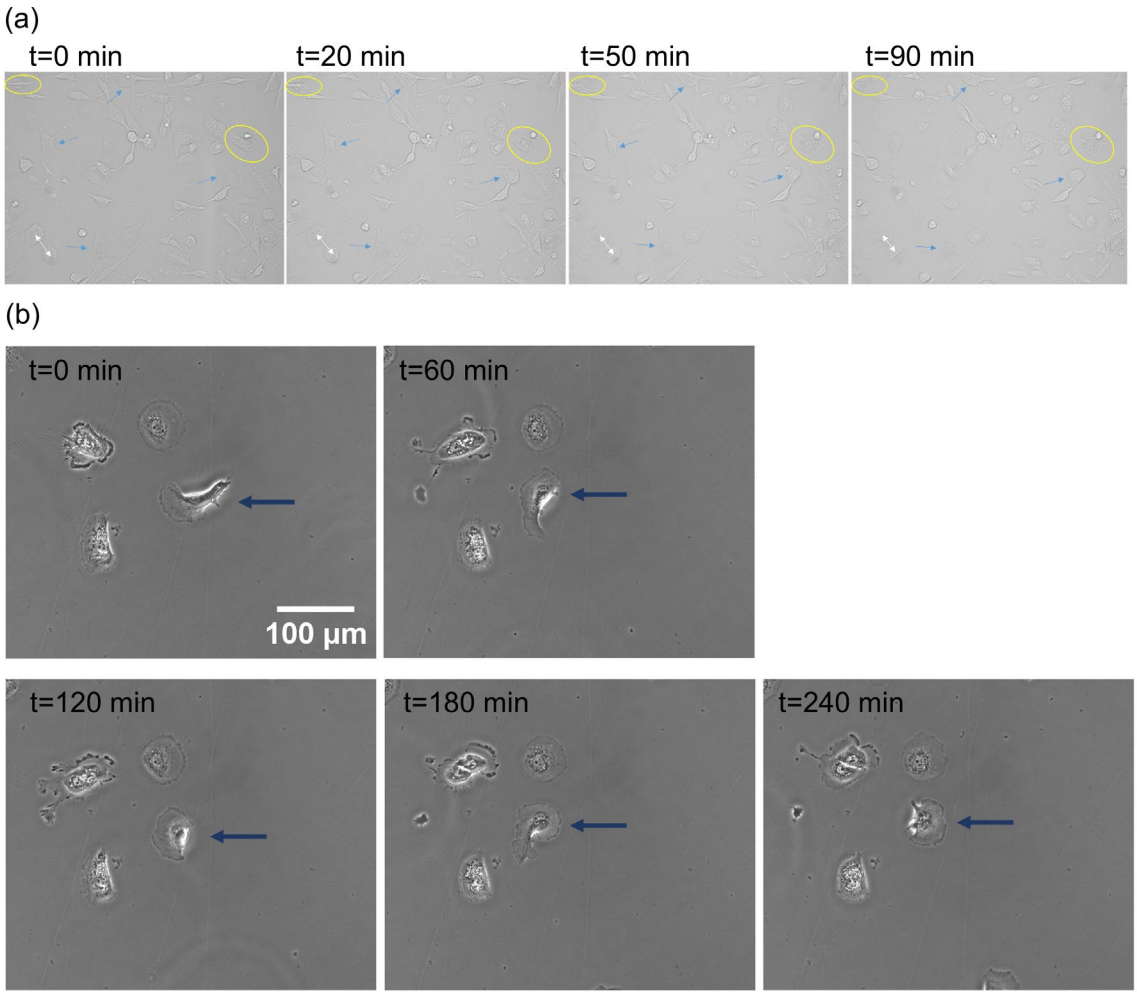

Figure S2 (a) Time series of optical microscopy images of breast cancer cell, the shrink and expansion of cell sizes were observed with low resolution (see arrows, circles). (b) Time series of phase-contrast microscopy images at room temperature without CO_2 control. Some cells were surrounded with fuzzy fringes. The migration was observed (see blue arrows). Lamellipodia or microvilli could not be observed.

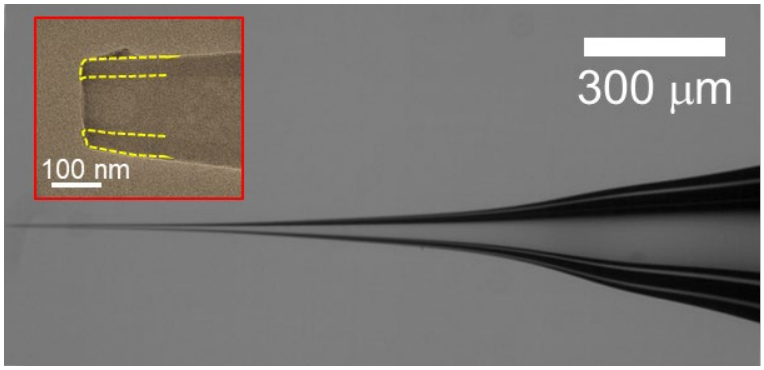

Figure S3 Geometrical characterization of nanopipette by optical microscopy and TEM (inset) measurements

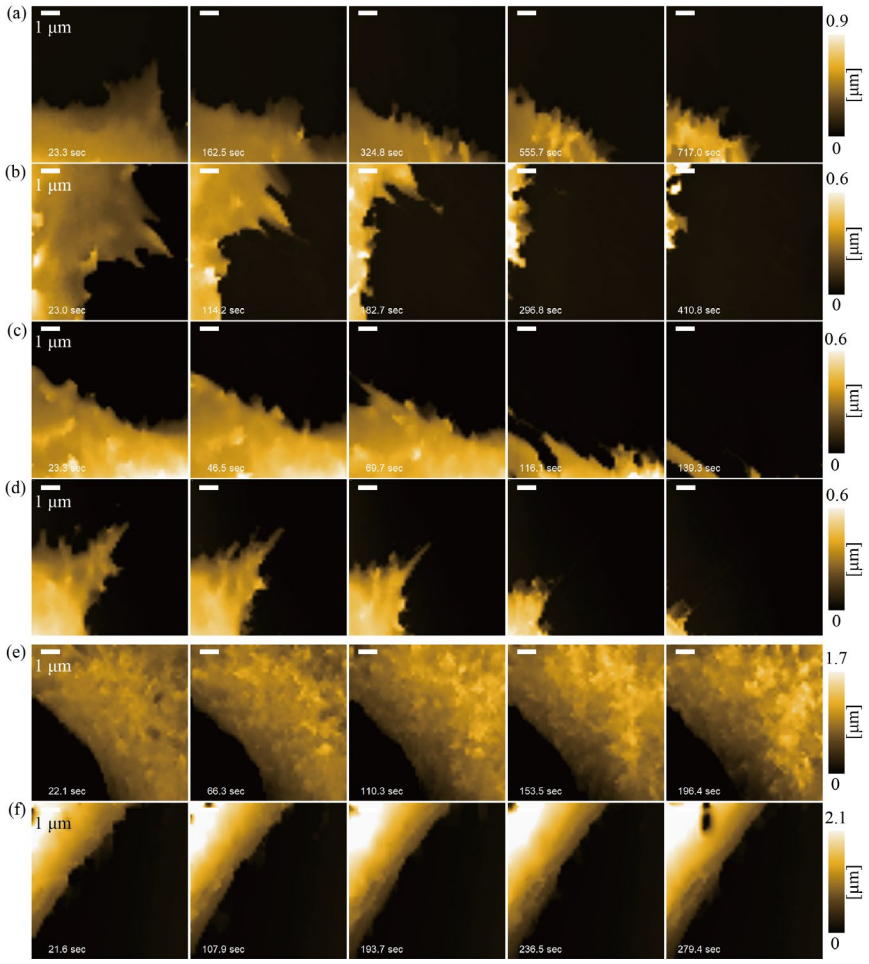

Figure S4 Dynamical observations of cell edge with filopodia (a-d) and without filopodia (e-f)

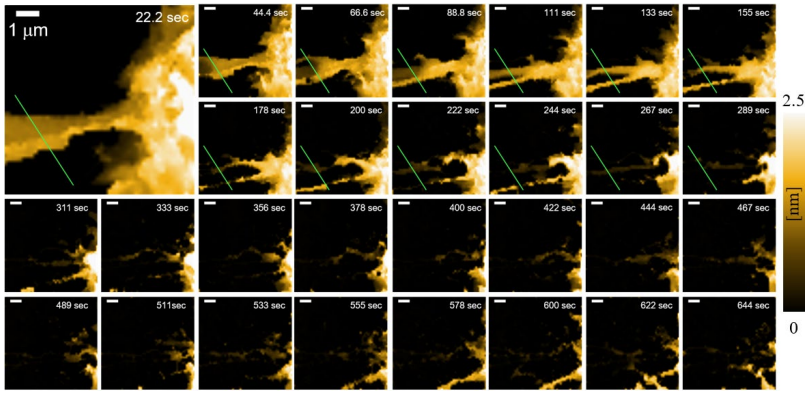

Figure S5 Filopodium structural dynamics revealed by SICM measurements. The time-dependent height profiles were analyzed crossing the same location of filopodium structures as shown in Figure 2c.

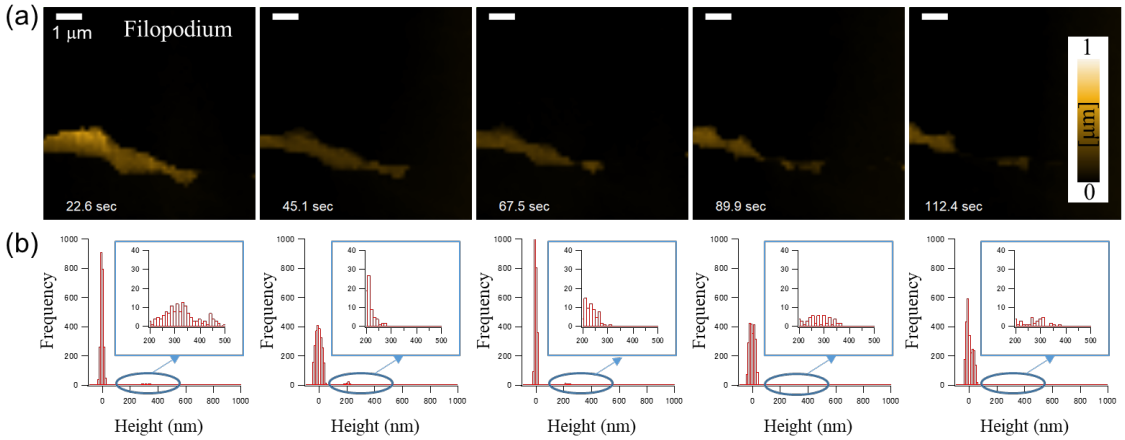

Figure S6. (a) Time series of SICM topographic images of filopodium and (b) corresponding height distribution.

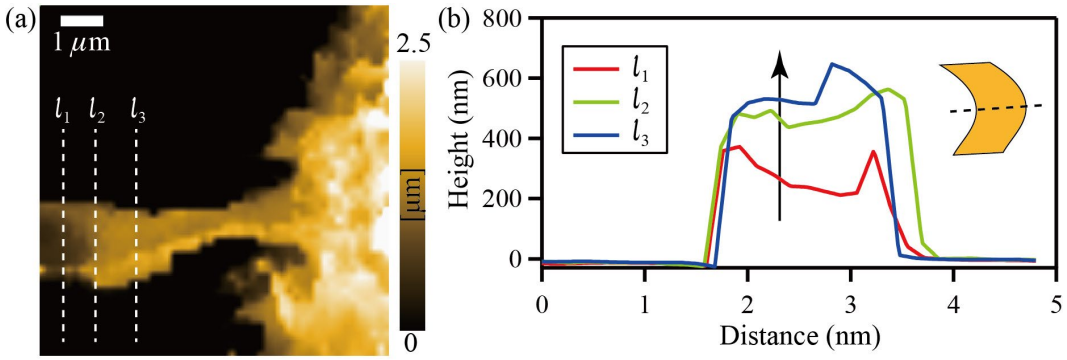

Figure S7 (a) SICM image containing filopodium structures from Figure 2a (Frame 2). (b) Line profiles crossing filopodium structure corresponding to the lines 1 to 3.

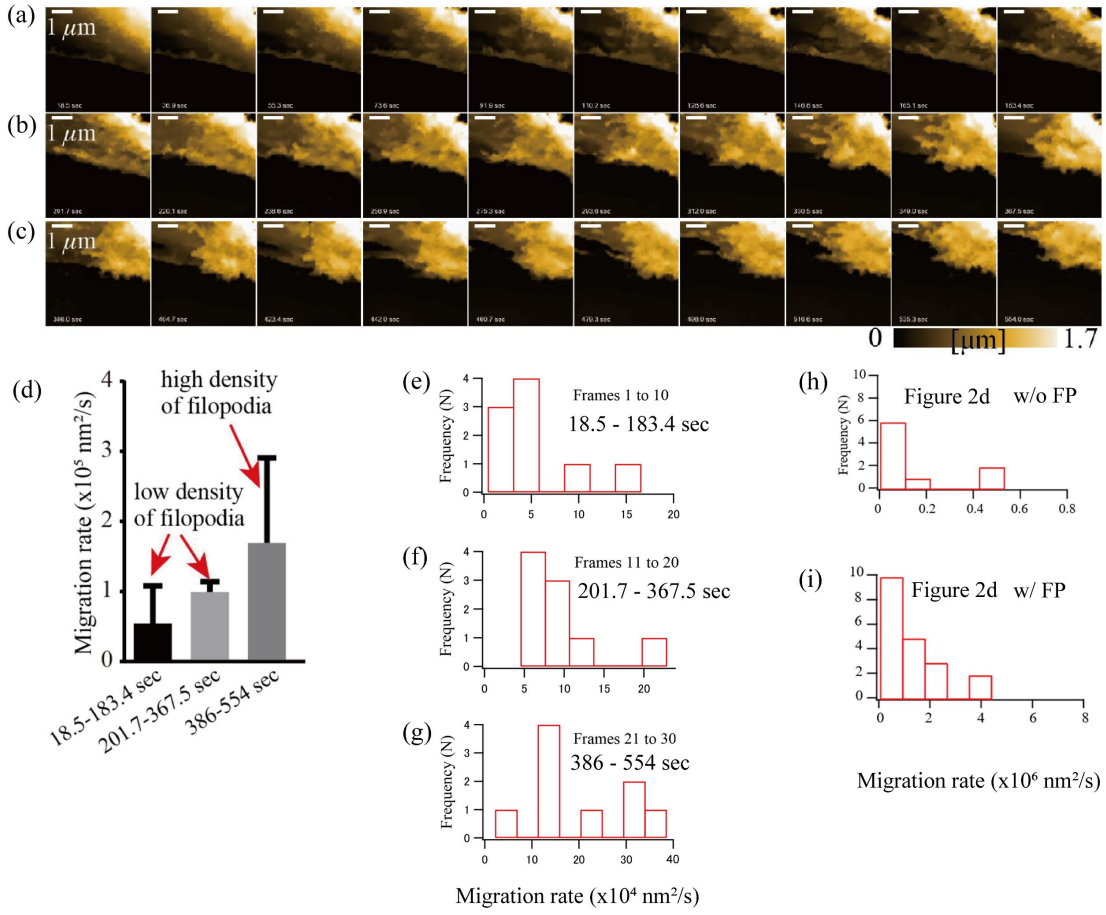

Figure S8 (a) Local migration rates with and without filopodial structures. Noticeable filopodial structures were not observed in SICM images from 18.5 to 183.4 s (w/o FP). (b) Tiny filopodia were observed in images taken from 201.7 to 367.5 s. (c) Apparent filopodia were observed in images taken from 386 to 554 s. (e–g) Histograms of migration rates extracted from (a), (b), and (c), respectively. (h, i) Histograms of migration rates shown in Fig. 2d of the main text.

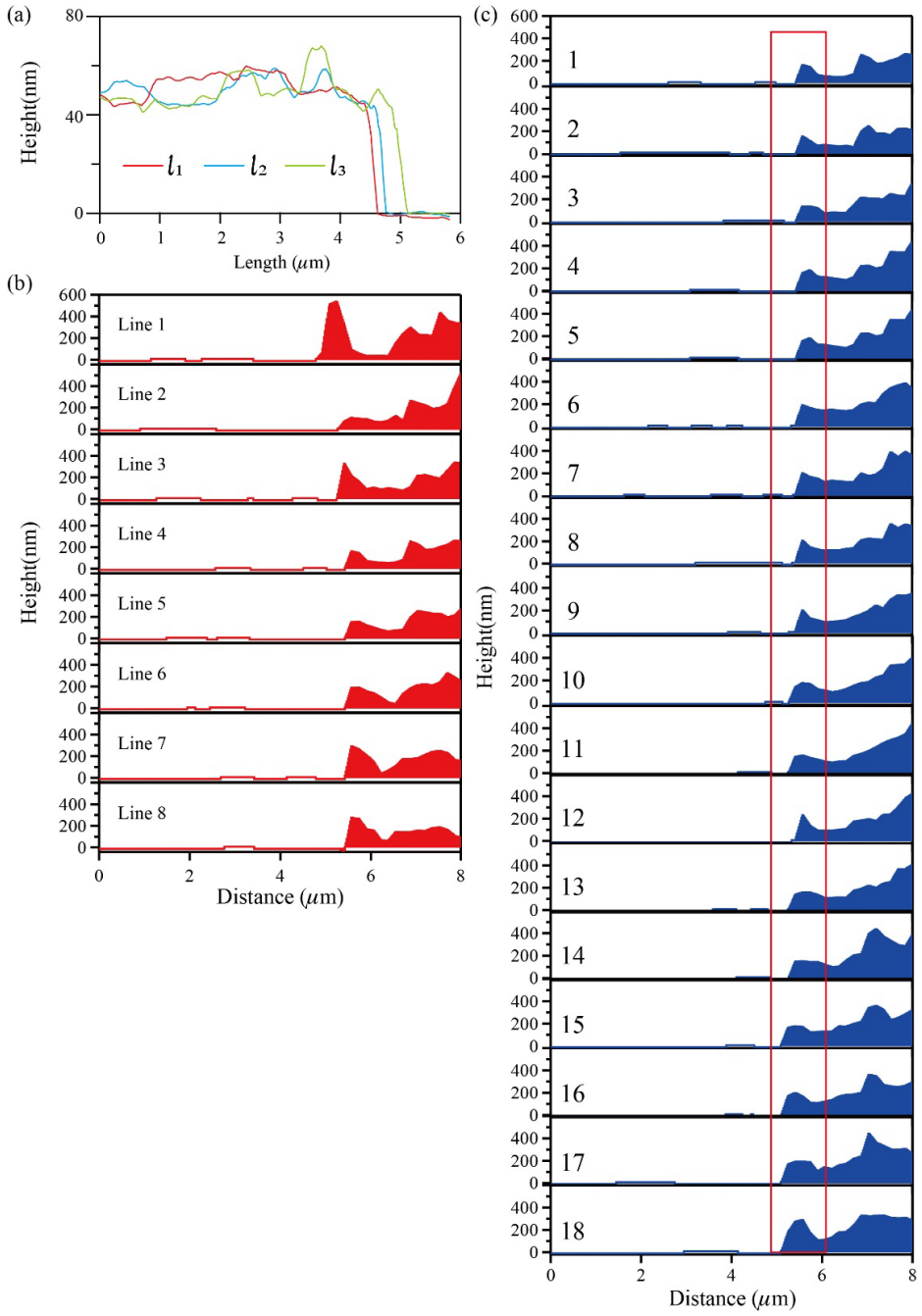

Figure S9 (a) Height profiles of the lamellipodia structure along lines l_1 to l_3 in frame 1 of Figure 3a in the main text. (b) Height profiles of the cell membrane along dashed white lines L_1 to L_8 in Figure 3c, identical to the data in Figure 3f. (c) Height profiles along green lines in Figure 3c from frames 1 to 18, identical to the data in Figure 3g. The red square area in (c) displays the data shown in the inset of Figure 3f.

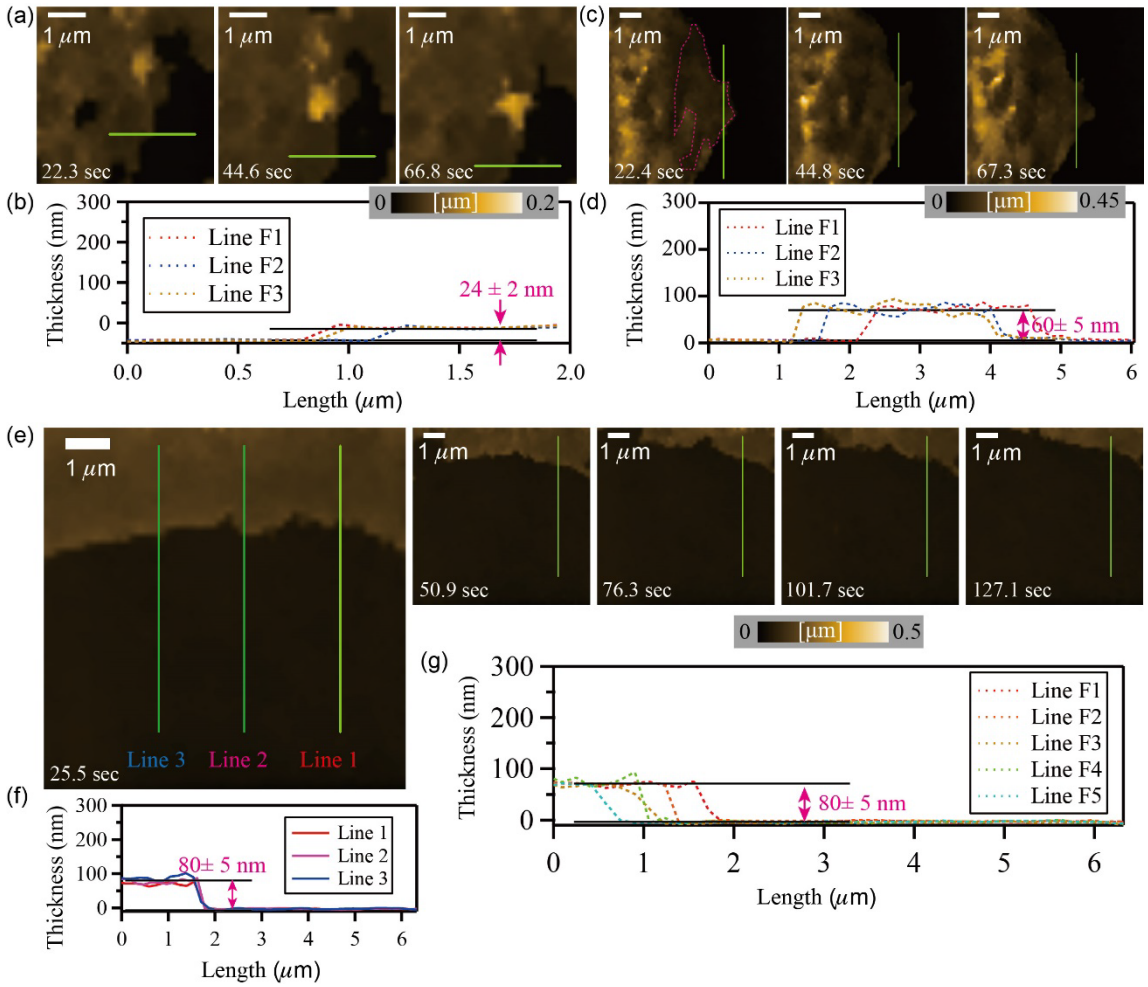

Figure S10 Lamellipodia structures with thin thickness. (a, b) Lamellipodia with thickness of 24 ± 2 nm, (c, d) Lamellipodia with thickness of 60 ± 5 nm, the red dashed curve in topographic image indicating the lamellipodia structure. (e, f, g) Lamellipodia with thickness of 80 ± 5 nm examined at different locations and timescale.

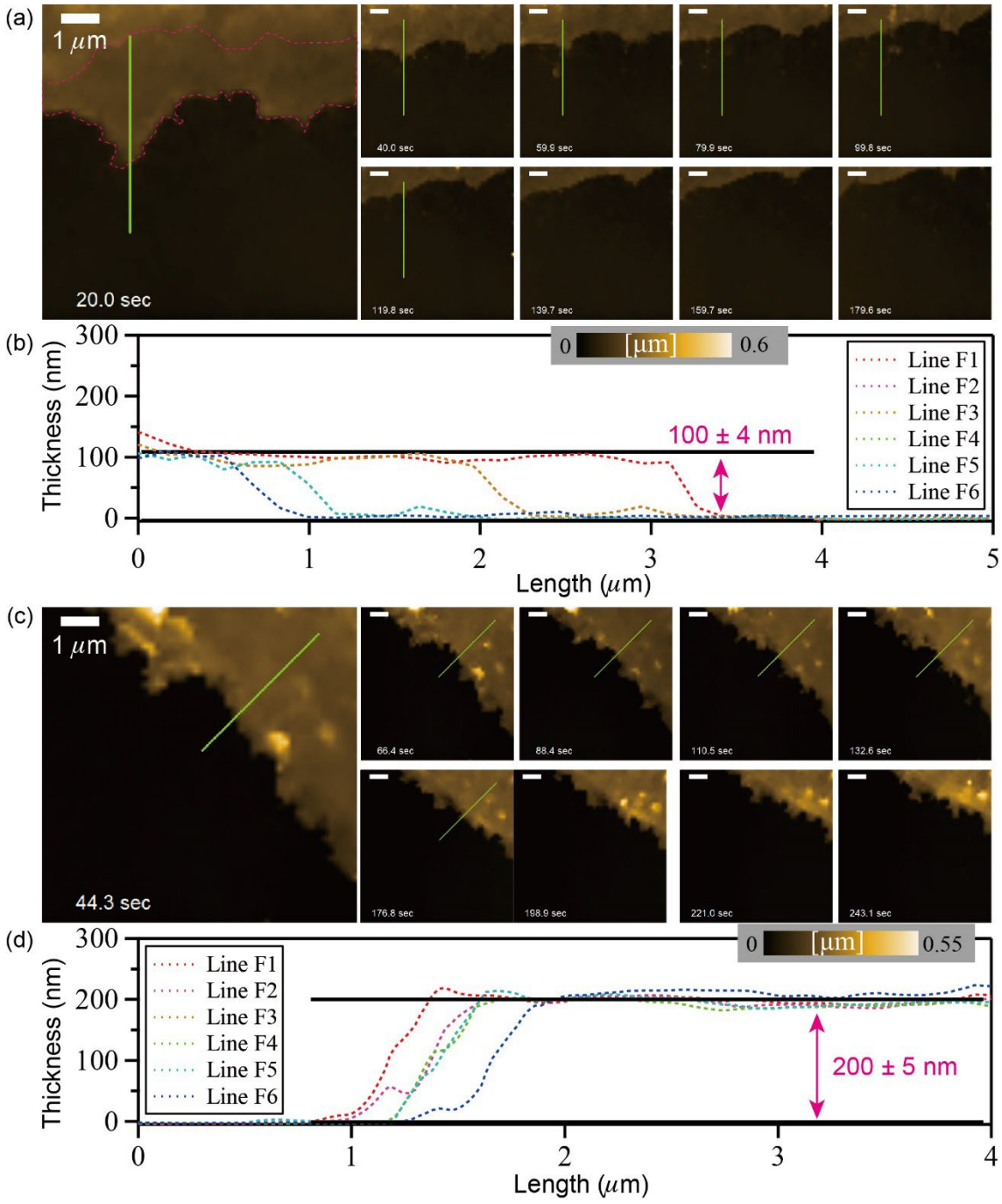

Figure S11 Lamellipodia structures with thick thickness. (a, b) Lamellipodia with thickness of 100 ± 4 nm, (c, d) Lamellipodia with thickness of 200 ± 5 nm, the red dashed curve in topographic image indicating the lamellipodia structure.

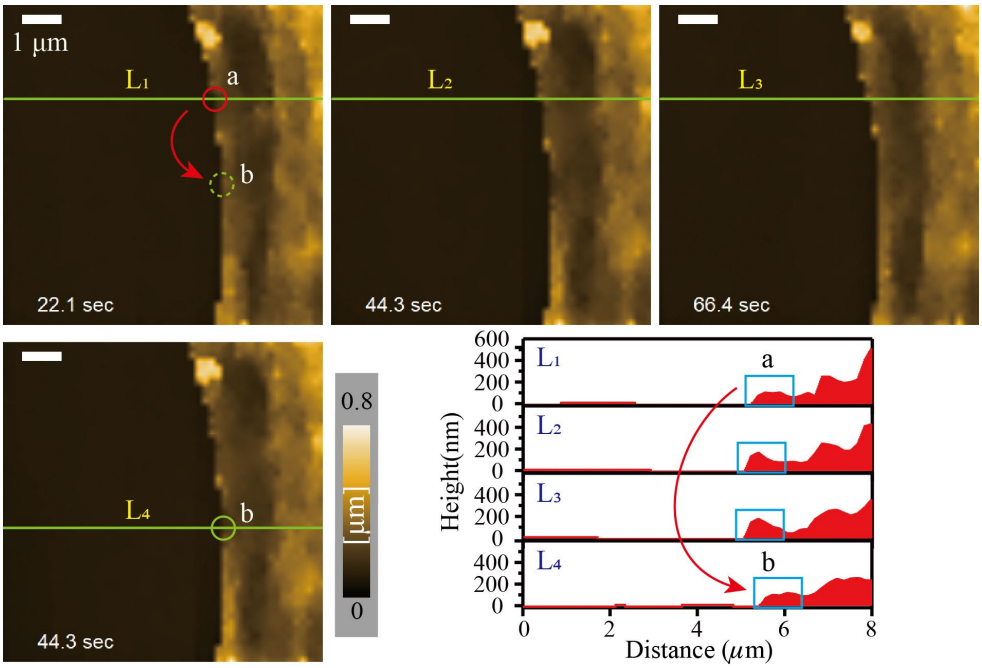

Figure S12 Height profiles of cell edge without lamellipodia structures.

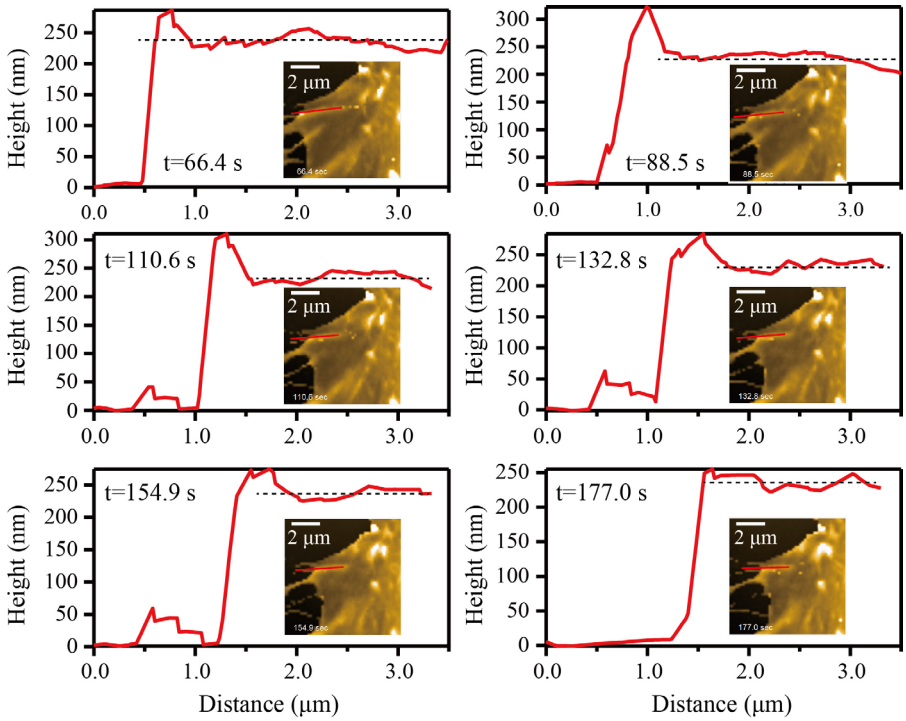

Figure S13 Height profiles along linear ridge-like structures.

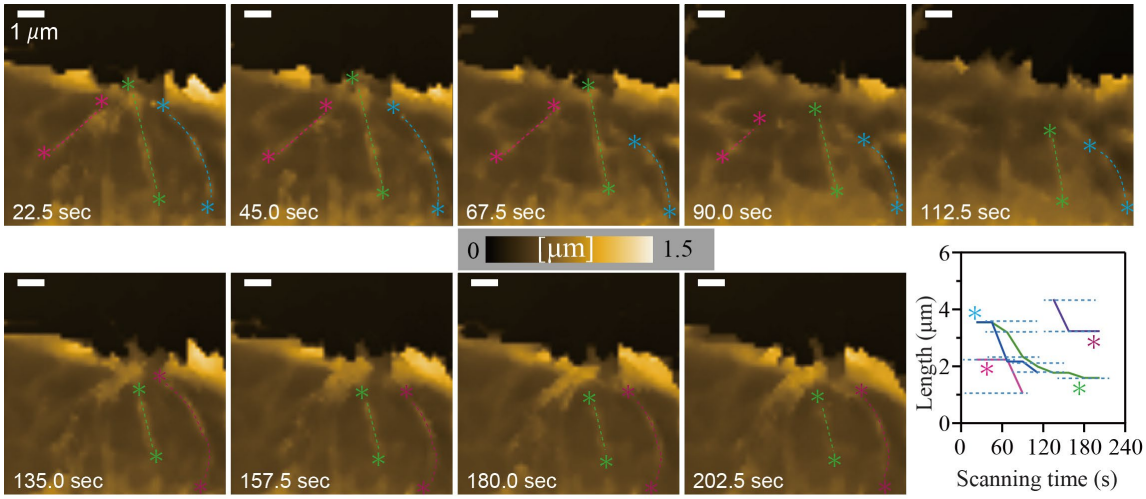

Figure S14 Time-lapse SICM images to track the cytoskeleton length changes around the cell edge.

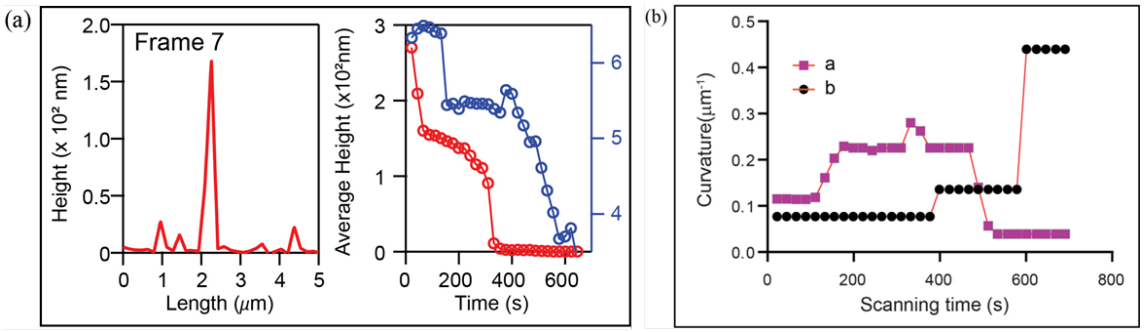

Figure S15 (a) Height profiles of filopodia structures, (b) Curvature changes of cell edge with scanning time.

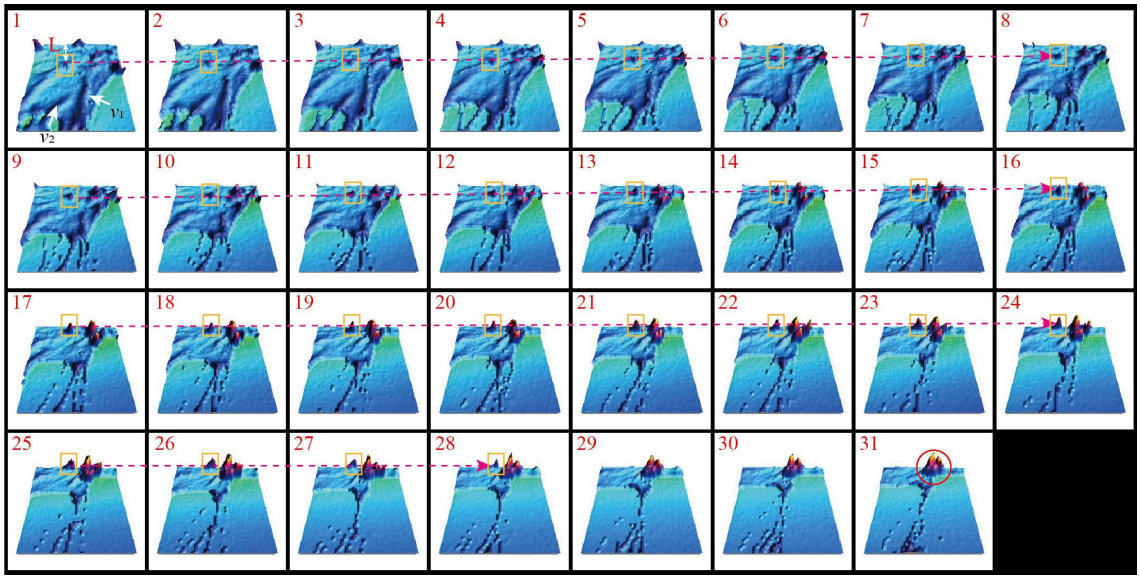

Figure S16 Dynamics of microstructures induced by cytoskeletal filaments, as visualized in 3D images corresponding to the topographic images in Figure 4

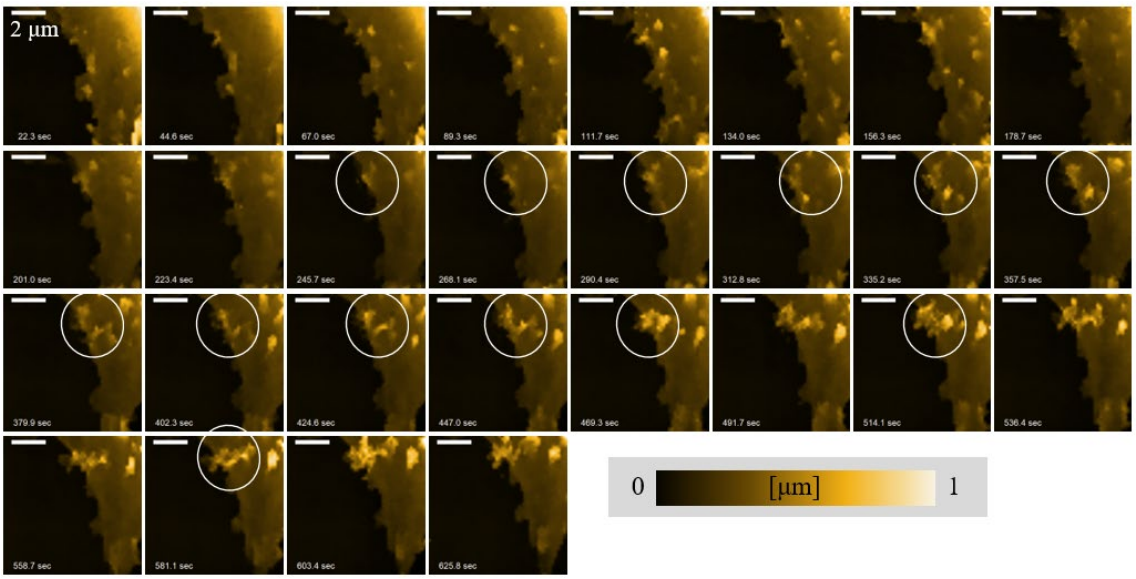

Figure S17. Dynamical observations for the reversible formation and decomposition of pore-like microstructures by SICM. The white circles from time series SICM images recorded the pore formation and decomposition processes.

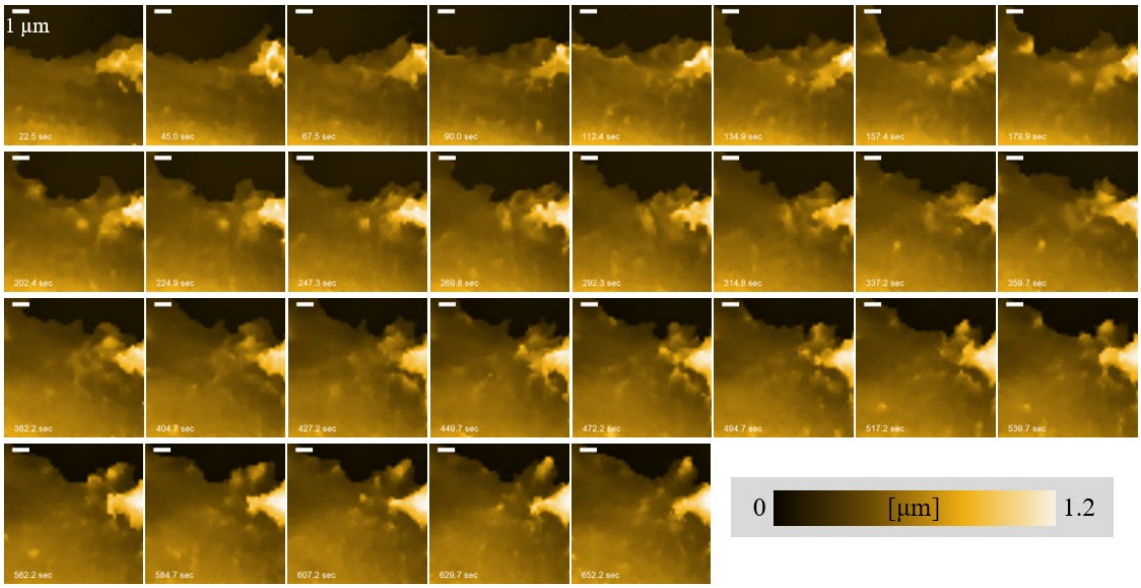

Figure S18 Morphological dynamics of filopodium and pore-like microstructures at the leading edge of living cell.

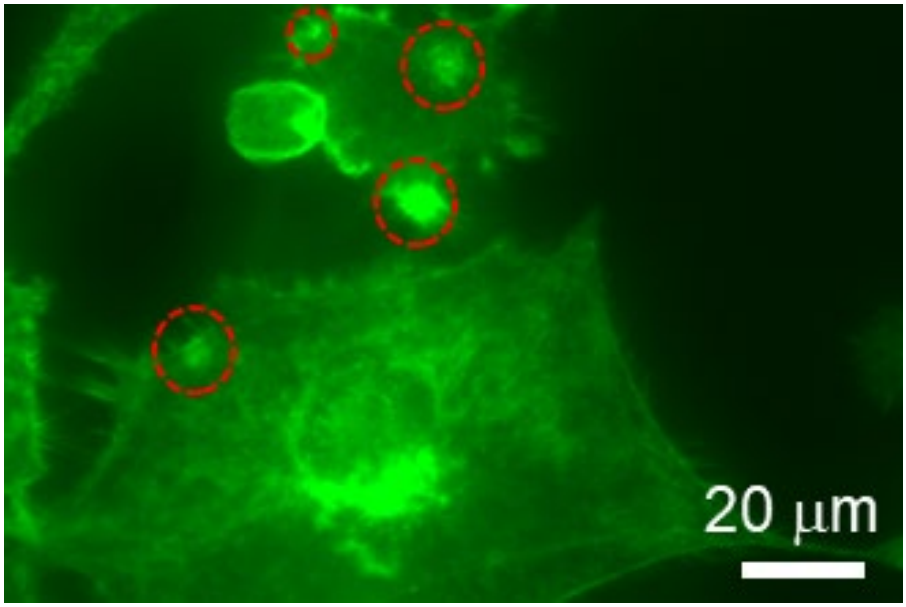

Figure S19 Formation of pore-like microstructures induced by cytoskeleton filaments taken by fluorescence microscopy.

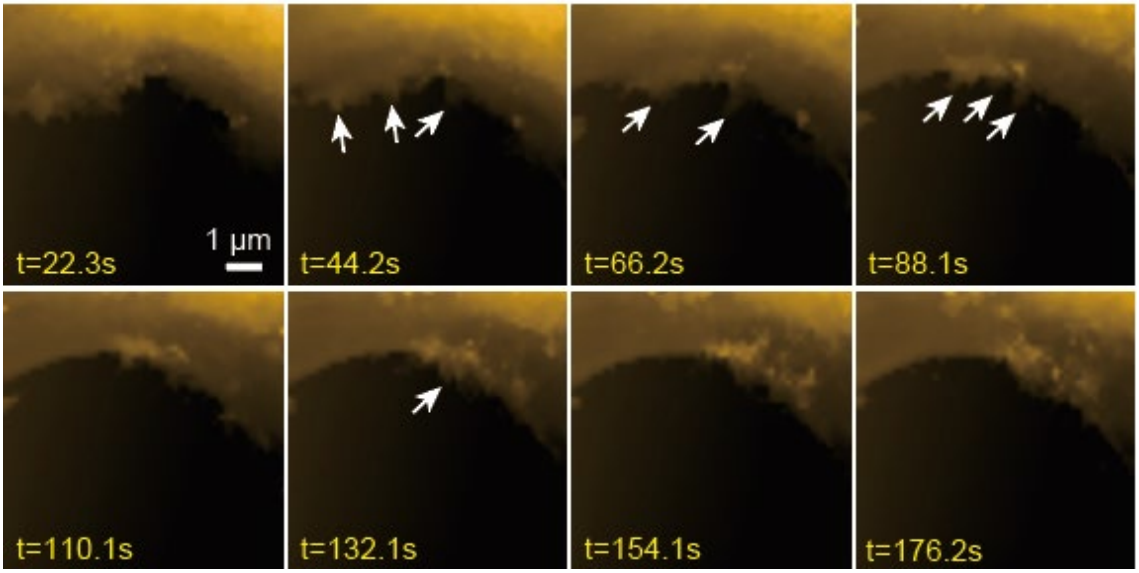

Figure S20 Membrane dynamics in tumour cells without ionizing radiation.

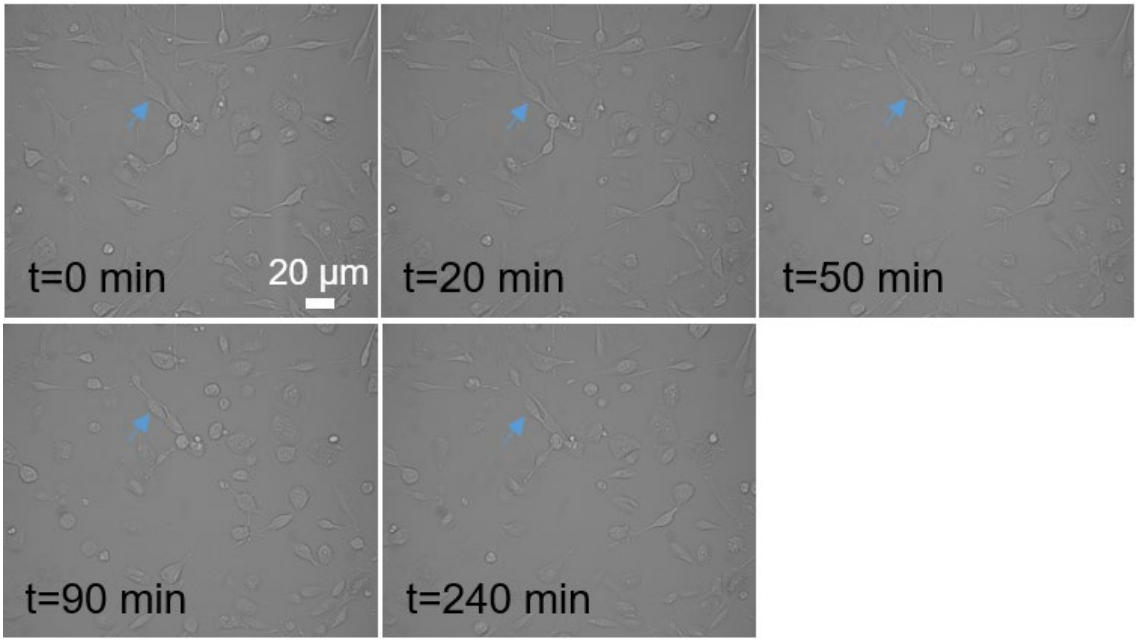

Figure S21 Time-lapse OM images after SICM imaging. The cells in EpiCult^{TM}-C medium (Human) were observed at room temperature without CO_2 control. A cell marked by blue arrows was imaged by SICM under a 3% setpoint reduction. After 4 hours of observation, the cell did not show cell-death signs, such as several notches on the cell outline and cell floating.

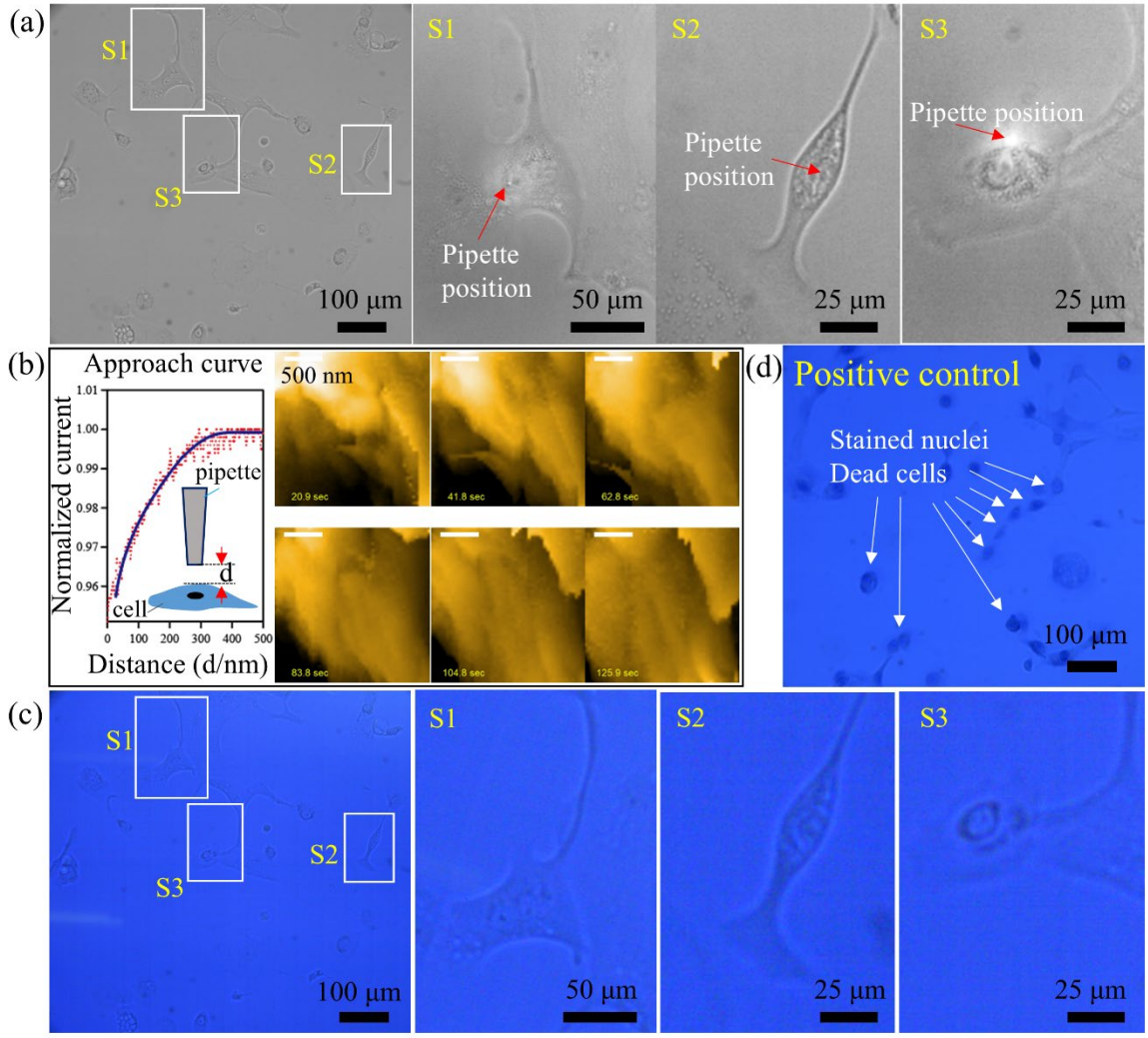

Figure S22 Cell viability after SICM imaging without CO_2 control at room temperature using a 3–4% setpoint value. (a) Optical microscopy images showing nanopipette positions over three cell surfaces (S1, S2, and S3). (b) An example of an approach curve demonstrating a ~4% setpoint threshold, along with corresponding time-lapse SICM images. (c) Cell viability was assessed using a trypan blue assay. Trypan blue was applied 1 hour after SICM measurements. The nuclei of the cells scanned by SICM did not take up the dye, suggesting that the cells remained viable. (d) Representative images of dead cells are shown (white arrows). The nuclei were clearly stained blue. Viability was tested 1 hour after exposure to 30% dimethyl sulfoxide as a positive control.

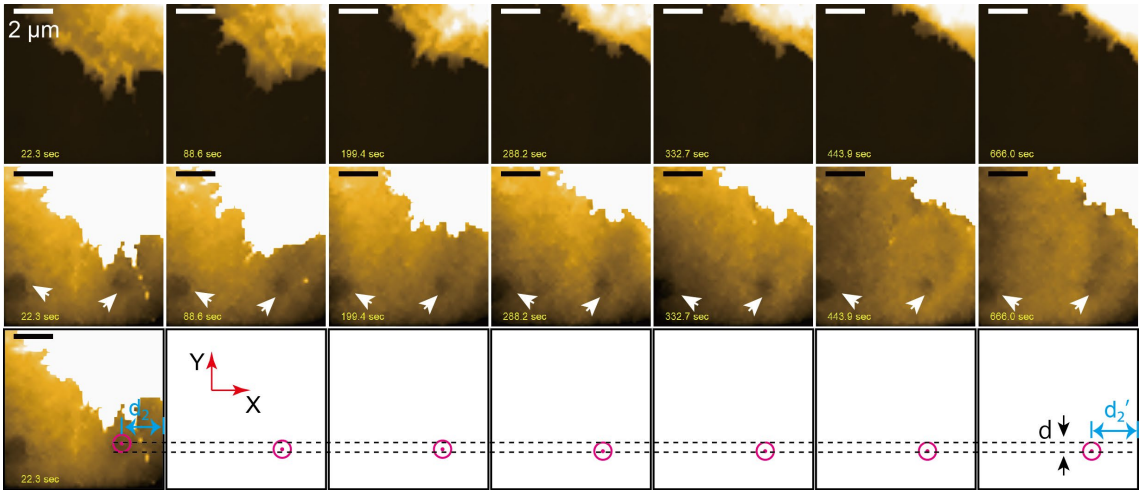

Figure S23 Estimation of drift effect. Here, we demonstrate how to estimate the drift effect from time-lapsed SICM images of cell edges. The first row shows the time-lapse SICM images of the cell edge. The second row contains the same images as the first row, but with adjusted contrast to enhance certain patterns (white arrowheads) on the substrate. These patterns can be used as markers to estimate drift size, as they remain independent of cell movement. We calculated marker displacement, as shown in the third row, where selected markers are indicated as pink circles. The drift rates along the X and Y directions were determined to be 0.33 and 0.73 nm/s, respectively. The drift over 660 s in the X and Y directions is indicated as d, and the difference of d2 and d2' in the third row. The measured drift rate is at least five orders of magnitude smaller than the migration rate of cells, indicating that the drift effect is negligible.

Table S1 Pulling parameters for fabrication of nanopipettes

HEAT	FIL	VEL	DEL	PUL
350	0	10	110	20
400	0	10	185	190

References

(1) Linz S, Willman E, Caldwell M, Klenerman D, Fernandez A, Moss, G. Contact-Free Scanning and Imaging with the Scanning Ion Conductance Microscope. 2014**, 86** (5), 2353-2360.

(2) Shigyou, K.; Sun, L.; Yajima, R.; Takigaura, S.; Tajima, M.; Furusho, H.; Kikuchi, Y.; Miyazawa, K.; Fukuma, T.; Taoka, A. Geometrical Characterization of Glass Nanopipettes with Sub-10 Nm Pore Diameter by Transmission Electron Microscopy. *Analytical Chemistry* 2020, **92** (23), 15388–15393.